Microstructure and dielectric properties with CuO additions to liquid phase sintered $BaTiO_3$ thin films

David T. Harris,[a] Matthew J. Burch, Edward J. Mily, Elizabeth C. Dickey, and Jon-Paul Maria
Department of Materials Science and Engineering, North Carolina State University, Raleigh, North Carolina 27606, USA

(Received 21 December 2015; accepted 25 February 2016)

The refractory nature of $BaTiO_3$ leads to limited densification and grain growth for films processed at low temperatures and a modest nonlinear dielectric response due to a marked sensitivity to physical scale and material quality. Adding liquid-forming sintering aids, common in bulk ceramics, to thin films enhances mass transport, leading to enhanced grain growth at lower temperatures. This work explores the effectiveness of a sputtered CuO buffer layer with $BaO–B_2O_3$ (BBO) fluxes to engineer the microstructure of $BaTiO_3$ films. Grain size and homogeneity increase in the presence of even a ~1 nm CuO layer. In general, grain size increases from 75 to 370 nm with an addition of 2.2% BBO and 8 nm CuO. Room temperature capacitance in fluxed films increases by a factor of 5 over pure films, and ferroelectric phase transitions are clearly observable in dielectric measurements. CuO–BBO proves effective on (0001) Al_2O_3 and (100) MgO substrates, although all microstructures are notably finer for the latter.

I. INTRODUCTION

The functional properties of oxides in ferroelectric, ferromagnetic, optic, and other electronic devices promise enhanced performance and novel applications. However, large challenges exist when integrating certain oxide materials with thin film systems as a consequence of restricting thermal budgets to minimize chemical reactions and maximize substrate and electrode compatibility. Due to the sensitivity of $BaTiO_3$ to processing temperature,[1] carbon removal,[1,2] strain,[3,4] and physical scale,[1,2,5,6] this class of materials serves as a model system for understanding how refractory thin film oxide processing can be improved.

Adding sintering aides to multilayer ceramic capacitors reduces firing temperatures to levels compatible with alloyed or base-metal electrodes.[7] Liquid forming fluxes encourage densification and grain growth at lower temperatures for $BaTiO_3$-based materials and other refractory complex oxides.[8] Recently, liquid-phase work was extended to epitaxial films[9] and polycrystalline $Ba_{1-x}(Sr_x)TiO_3$ films[10–12] grown using chemical solution deposition, radio frequency (RF)-magnetron sputtering, and pulsed laser deposition. Densification and grain growth occurs at significantly lower temperatures, improving the dielectric and ferroelectric properties of these complex oxide systems without increasing the thermal budget. However, for $BaTiO_3$-thin films, the final average grain size is limited to around 300 nm, with further flux additions leading to deteriorated properties or abnormal grain growth and heterogeneous microstructures.

Burn[13] and Hennings[14,15] first recognized combinations of copper oxide and other modifiers as effective sintering aides for $BaTiO_3$. Both authors reported densification by 1100 °C, but explorations of the dielectric properties were initially limited. Later studies isolated CuO (Ref. 16) and CuO–BaO,[17] again demonstrating substantial grain growth at lower temperatures, with appreciable improvements to the dielectric constant. In this report, CuO additions to the $BaTiO_3$ with and without $BaO–B_2O_3$ (BBO) are studied using pulsed laser deposition. CuO is added to the system in the form of a thin buffer layer sputtered on the substrates prior to $BaTiO_3$ deposition. Addition of CuO or CuO + BBO to $BaTiO_3$ films encourages densification and grain growth and realizes large improvements to the linear and nonlinear dielectric properties.

II. EXPERIMENTAL PROCEDURE

CuO buffer layers were deposited using RF-magnetron sputtering at room temperature from a commercial 2-in. CuO target (Kurt J. Lesker, Pittsburgh, Pennsylvania). A pre-sputter of 10 min in 12 mTorr Ar was followed by CuO film deposition using a power of 100 W, a target–substrate distance of 7 cm, and an atmosphere of 5 mTorr Ar. The deposition rate was calibrated to 17 nm/min and the deposition time was varied to control the CuO buffer layer thickness.

Thin films were prepared from pure $BaTiO_3$ or $BaTiO_3$ targets containing 2.2% by mass of BBO 869 °C eutectic

Contributing Editor: Ian M. Reaney
[a]Address all correspondence to this author.
e-mail: david.harris@wisc.edu
DOI: 10.1557/jmr.2016.89

 © Materials Research Society 2016

https://doi.org/10.1557/jmr.2016.89 Published online by Cambridge University Press

composition flux on various CuO buffered and unbuffered substrates using pulsed laser deposition (Coherent Compex Pro 102 F; KrF laser $\lambda = 248$ nm). The BBO flux was synthesized using chemical solution precipitation[11] and ball milled with commercial $BaTiO_3$ (Sakai Trading Company, Osaka, Japan; high purity perovskite BT-01) before pressing and sintering in air at 1100 °C for 1 h. The laser fluence was 1.5 J/cm^2, the laser repetition rate 7 Hz, the target–substrate distance was 7.5 cm, the substrate temperature was held at 400 °C to promote dense deposition, and the ambient atmosphere was held at 30 mTorr O_2. Post deposition crystallization was performed in air in a tube furnace. All films, regardless of the substrate, were processed and characterized identically. (0001) *c*-Sapphire substrates were purchased from Jiaozuo City Crystal Photoelectric Material Co., Ltd. (Jiaozuo, China). (100) MgO substrates were purchased from CrysTec (Berlin, Germany).

Microstructure characterization was performed using an FEI Verios field-emission scanning electron microscope (FE-SEM; FEI Company, Hillsboro, Oregon). Grain size measurements and distributions were performed using linear intercept stereology.[18] Dielectric properties were measured with a HP 4192A impedance analyzer (1 MHz; HP, Palo Alto, California) using 150 nm thick direct current (DC)-sputtered platinum interdigitated contacts defined via photolithography with a gap size of 2 μm, a gap length of 200 μm, and a total of 40 fingers. Temperature-dependent measurements were performed on a MMR Technologies (San Jose, California) miniature refrigerator stage starting at elevated temperatures with a ramp rate of −6 °C/min. Phase analysis of samples on sapphire was performed using x-ray diffraction (XRD) on a PANalytical Empyrean (Almelo, The Netherlands) with Bragg–Brentano geometry and a Cu–K_α source. For samples on MgO, the substrate reflections from the W emission in the x-ray source are substantially stronger. Therefore, XRD of samples on MgO was performed using a parallel beam hybrid double-bounce monochromator source with a parallel plate collimator on the detector that removes spectral reflections and $K_{\alpha 2}$ reflections.

Transmission Kikuchi diffraction was performed at 30 kV on a DualBeam FEI Quanta 3D FE-SEM using an Oxford Instruments NordlysNano electron backscatter diffraction (EBSD) detector (Abingdon, United Kingdom). Samples were prepared using focused ion beam (FIB) milling in the DualBeam FEI Quanta 3D

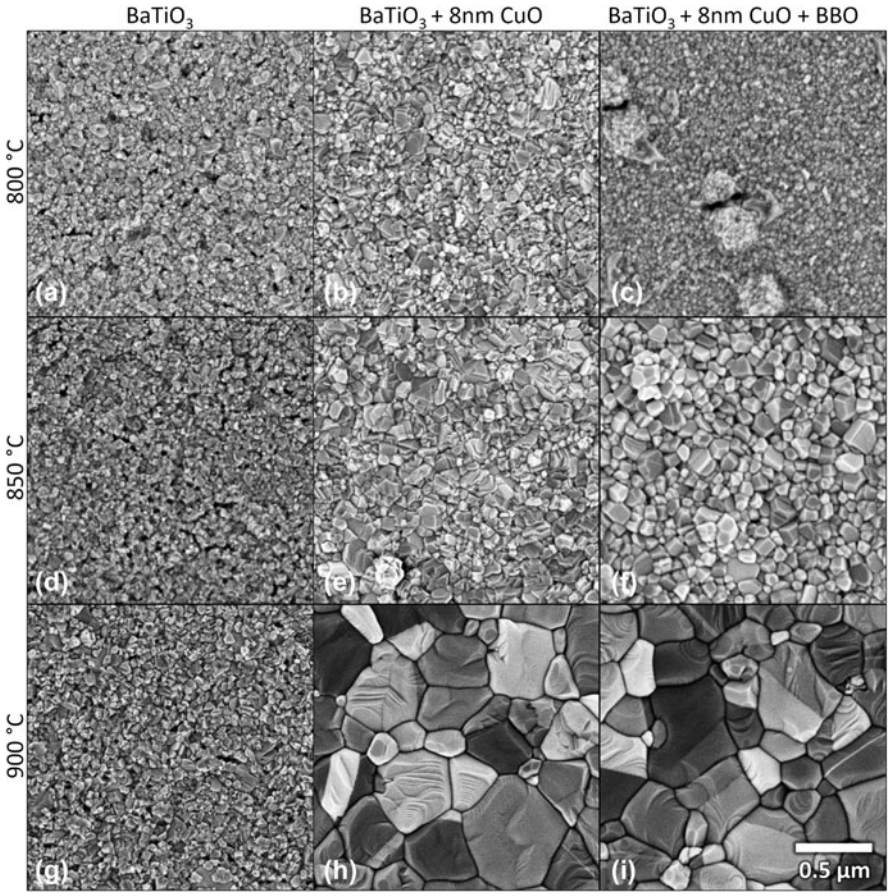


FIG. 1. SEM plan-view micrographs of [(a), (d), and (g)] pure $BaTiO_3$, [(b), (e), and (h)] $BaTiO_3$ + 8 nm CuO, and [(c), (f), and (i)] $BaTiO_3$ + 8 nm CuO + 2.2% BBO on *c*-sapphire annealed at 800, 850, and 900 °C in air.

https://doi.org/10.1557/jmr.2016.89 Published online by Cambridge University Press

FEG-SEM/FIB. Postprocessing and map creation of the transmission Kikuchi diffraction data was performed on Oxford Instruments Aztec software and the HKL CHANNEL5 program Tango.

TABLE I. Average grain sizes of films annealed at 900 °C (above the liquid-forming temperature).

Substrate	BBO inclusion (%)	CuO thickness (nm)	Average grain size (nm)	Grain size standard deviation (nm)
Sapphire	0	0	75	35
Sapphire	0	8	380	210
Sapphire	2.2	0	290	210
Sapphire	2.2	1	370	190
Sapphire	2.2	8	370	180
Sapphire	2.2	100	660	340
MgO	0	0	58	26
MgO	0	8	93	57
MgO	2.2	8	190	92

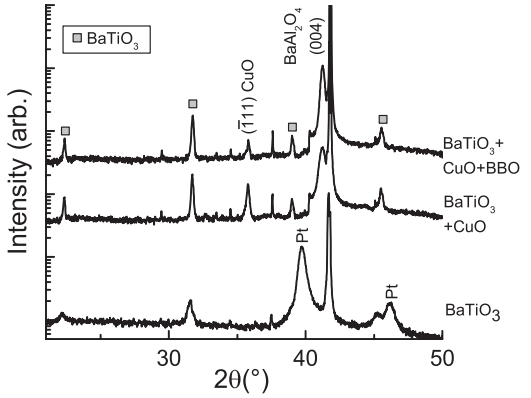


FIG. 2. XRD patterns of $BaTiO_3$ on *c*-sapphire annealed at 900 °C with 8 nm CuO and 8 nm CuO + 2.2% BBO additions. The pure $BaTiO_3$ sample includes Pt top electrodes. Unlabeled peaks are due to substrate reflections.

III. RESULTS AND DISCUSSIONS

A. Growth on *c*-sapphire

Figure 1 shows a compilation of SEM plan-view images of barium titanate films without additions, with a sputtered 8 nm CuO buffer layer, and with an 8 nm CuO buffer and BBO. The three different sets were annealed at 800, 850, and 900 °C in air for 1 h for crystallization, densification, and grain growth. As expected, pure $BaTiO_3$ exhibits limited grain growth and only minor densification at the temperatures studied. Adding an 8 nm CuO buffer layer prior to $BaTiO_3$ deposition results in densification and grain growth at 800 °C, with higher temperatures leading to a substantially coarser microstructure. At 800 °C, $BaTiO_3$ + BBO deposited on 8 nm of CuO appears dense, but with a finer microstructure than with the CuO layer alone. Annealing at 900 °C, above the expected liquid formation temperatures in these systems,[19,20] leads to substantial grain growth. The final microstructures of $BaTiO_3$ + CuO with and without BBO appear similar in density and grain size. After annealing at 900 °C, the average grain size increases from 75 nm in pure $BaTiO_3$ to 380 or 370 nm with 8 nm CuO or CuO + BBO. Table I summarizes the average grain size and standard deviations for samples processed above the liquid forming temperature in these systems.

Figure 1(c) shows round ~100 nm hillocks, as well as nearby areas of an additional second phase, that are present after annealing samples containing both CuO and BBO at 800 °C or lower. These second phases are not present in the $BaTiO_3$ or $BaTiO_3$ + CuO systems, indicating that this feature likely arises from CuO–BBO interactions. When annealed at 800 °C, XRD reveals only

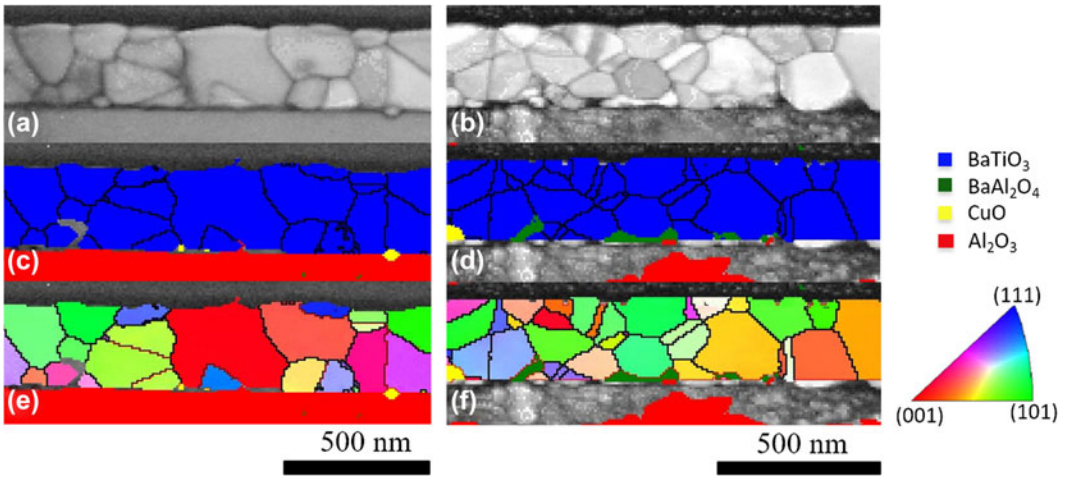


FIG. 3. Transmission Kikuchi diffraction maps of $BaTiO_3$ thin films with [(a), (c), and (e)] 8 nm of CuO present during growth and a thin film with [(b), (d), and (f)] 8 nm of CuO and 3% BBO flux present during growth. Parts (a) and (b) are the band contrast images of the respective thin films; (c) and (d) are the phase maps, which shows the presence of the $BaTiO_3$, Al_2O_3, CuO, and $BaAl_2O_4$; (e) and (f) are the crystallographic orientation maps showing the orientation of each grain (relative to the page normal) with the orientation of $BaTiO_3$ grains given by the inverses pole figure legend to the right.

https://doi.org/10.1557/jmr.2016.89 Published online by Cambridge University Press

the *c*-sapphire substrate, $BaTiO_3$, and a strong CuO peak, indicating that the round features are possibly due to de-wetting of liquid phases prior to reaction with $BaTiO_3$. Upon heating to higher temperatures, these hillocks disappear [Figs. 1(f) and 1(i)] and the intensity of the $(\bar{1}11)$ CuO XRD peak lessens (not shown), indicating loss of texture or incorporation into other phases.

XRD patterns of the samples annealed at 900 °C are shown in Fig. 2. Both of the systems that include CuO exhibit stronger and sharper $BaTiO_3$ peaks that are consistent with the large increase in grain size. A strong reflection matching $(\bar{1}11)$ CuO indicates its presence in both systems. In the as-deposited $BaTiO_3$ diffraction patterns, this peak is also present, but is significantly weaker and broader after annealing. The strength of the diffraction peak and fact that only members of the $(\bar{1}11)$ family are present indicate that during heating or $BaTiO_3$ deposition, the CuO becomes highly oriented. The presence of the (004) peak of $BaAl_2O_4$ is also of interest. Previous work showed that $BaAl_2O_4$ forms via an interface reaction when $BaTiO_3$ is prepared on *c*-sapphire, and this phase formation is accelerated in the presence of the flux.[21] Note that this interface phase will lead to a Ti-rich $BaTiO_3$ composition in the films without BBO.

Transmission Kikuchi diffraction from CuO-containing films with and without BBO flux is shown in Fig. 3. Linear stereology of available cross-sections yields average grain sizes in agreement with the plan-view SEM, however caution should be exercised in this analysis due to the significantly smaller population size of the cross-sections. The images reveal that the second phases observed in x-ray scans are located at the film–substrate interface. Both films contain residual areas of CuO in the form of small interface grains, suggesting de-wetting. The phase map [Fig. 3(d)] of the sample containing both CuO and BBO shows $BaAl_2O_4$ single crystal grains consistent with previously reported transmission electron microscopy (TEM) analysis,[11,22] however the Kikuchi phase map of the film with only CuO [Fig. 3(c)] contains areas at the interface that cannot be indexed due to low pattern quality. The patterns from these regions are consistent with, and likely to be $BaAl_2O_4$, with very fine grain size, or with substantial crystallographic disorder, as $BaAl_2O_4$ is observed in the x-ray patterns for the same samples. The large un-indexed area beneath the $BaTiO_3$ thin film with BBO is believed to arise from a region containing highly disordered alpha and gamma alumina resulting from the interface reaction.[21] The Kikuchi patterns from these regions are diffuse and indicate substantial crystallographic disorder, which leads to the low indexing rate. Crystallographic orientation maps [Figs. 3(e) and 3(f)] show the relative orientations of each grain and confirm the presence of twin boundaries that are also evident in the SEM images (Fig. 1).

The presence of $BaAl_2O_4$ has been shown to lead to {111} twin nucleation that drives abnormal grain growth in $BaTiO_3$.[22] These twin lamellae are also present in CuO-containing systems, and are shown in Figs. 1(h) and 1(i) as straight lines of contrast in several of the larger grains. The twin lamellae are apparent in

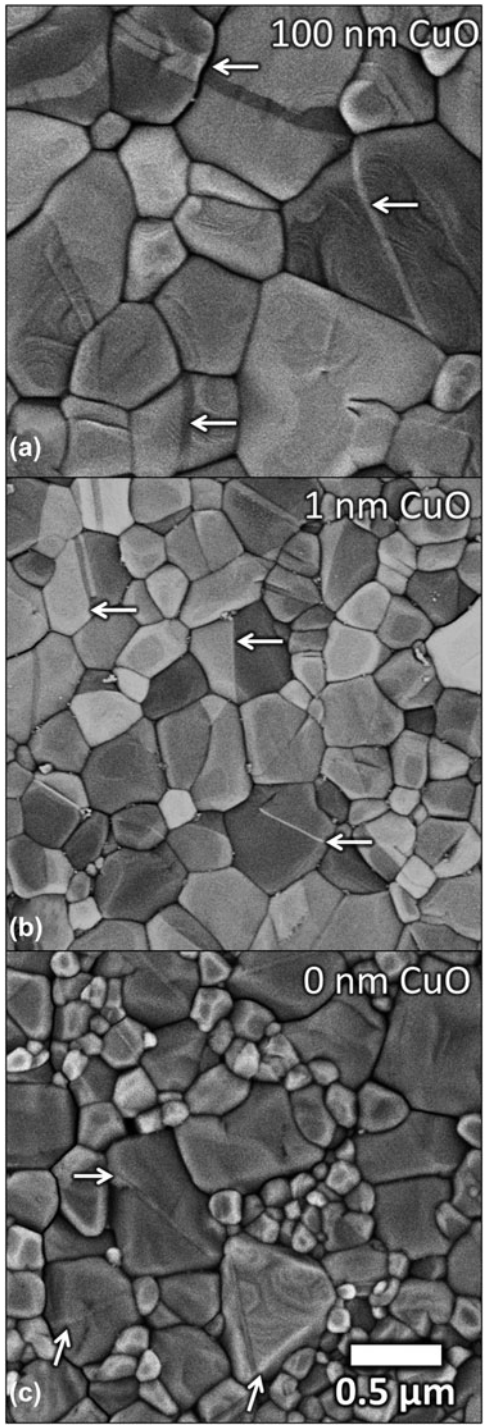


FIG. 4. SEM plan-view micrographs of pure $BaTiO_3$ + BBO on (a) 100 nm, (b) 1 nm, and (c) 0 nm of CuO annealed at 900 °C on *c*-sapphire. Example {111} twins are indicated by arrows.

https://doi.org/10.1557/jmr.2016.89 Published online by Cambridge University Press

the samples with and without BBO. To understand the impact of CuO on the microstructure, a series of films varying the amount of CuO was prepared and analyzed. Figure 4 shows SEM plan-view micrographs of $BaTiO_3$ + BBO deposited on CuO as a function of CuO layer thickness. In this experiment, all films containing CuO exhibit twin lamellae with an increasing prevalence for twinning with thicker CuO layers. While there is clear dependence on CuO thickness, adding even ~1 nm of CuO, as seen in Fig. 4(b), leads to additional grain growth and an overall microstructural homogenization when compared to $BaTiO_3$ + BBO. The average grain size of $BaTiO_3$ + BBO without CuO is 290 nm. This increases to 370 nm with 1 nm of CuO and to 660 nm with 100 nm of CuO.

To understand better how and when second phases evolve, we compare XRD and SEM data after the 900 °C anneals for samples with 8 nm CuO and 2.2% BBO. $BaAl_2O_4$ and CuO second phases are clearly discernible via XRD (Fig. 2). Figure 5(a) is a plan-view SEM micrograph that highlights the second phases that are apparent in these samples. For the sample with BBO and CuO [panel (a)], there are visible patchy regions whose smooth unfaceted morphology suggest a previously molten state. The segregation of these regions and the boundary curvature are consistent with poor wetting, and the previous studies of BaO–CuO on $BaTiO_3$ that found a contact angle of 42°.[23] Figure 5(b) shows a similar SEM image of $BaTiO_3$ + 8 nm CuO without BBO. These films did not contain the patchy, and likely glassy second phase regions, however there are small ~100 nm particles on top of $BaTiO_3$ grains and grain boundaries. While we do not know their composition, we speculate that they are Cu-containing.

In the related $BaTi_4O_9$ (Ref. 24) and $Ba(Zn_{1/3}Nb_{1/3})O_3$ (Ref. 25) systems, adding CuO–B_2O_3 sintering aides leads to a $BaCuB_2O_5$ intermediate at 850 °C and lower sintering temperatures. The BBO composition in our system forms a eutectic melt at 869 °C,[20] however CuO addition introduces additional possible melts involving $BaCuO_2$ or Ba_2CuO_3 near 900 °C.[19] XRD reveals no evidence for these crystalline second phases, and none match well with the $(\bar{1}11)$ CuO peak that is visible on samples both with and without BBO. Further obscuring our understanding is Al diffusion from the substrate.[21] Although no liquids are predicted to form below 1000 °C in the CuO–Al_2O_3 system,[26] no complete study of the aggregate Al–Cu–Ba–Ti–B–O system exists, complicating understanding of the exact mechanisms and possible liquids formed. However, interactions of BBO with CuO clearly lead to enhancement of grain growth, and, as will be discussed in detail later, removal of Al_2O_3 from the system reduces grain growth, suggesting that the combination of Cu and Al additions alter $BaTiO_3$ interactions with the BBO liquid.

While the BBO + CuO system shows promise for densification and grain growth, it is important to consider the impact on the dielectric response. To study the dielectric properties, capacitance as a function of temperature, shown in Fig. 6, was measured from films grown on *c*-sapphire and annealed at 900 °C. The use of surface interdigitated contacts makes reliable extraction of permittivity nontrivial, however as the film thicknesses and capacitor geometry were constant for all samples, the changes in capacitance are approximately proportional to changes in the thin film permittivity. In summary, adding an 8 nm CuO buffer layer to $BaTiO_3$ leads to a 3-fold increase in capacitance over the measured temperature

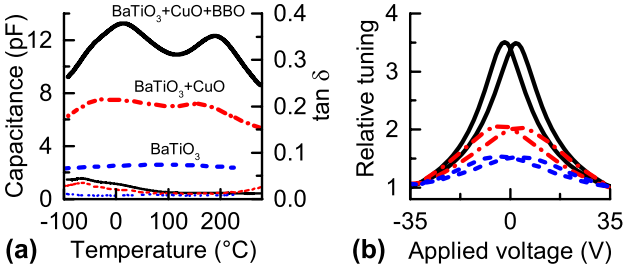


FIG. 6. (a) Capacitance and dielectric loss tangent versus temperature and (b) relative tuning with applied DC field after thermal de-aging for samples on *c*-sapphire annealed at 900 °C. Measurements were performed at 1 MHz.

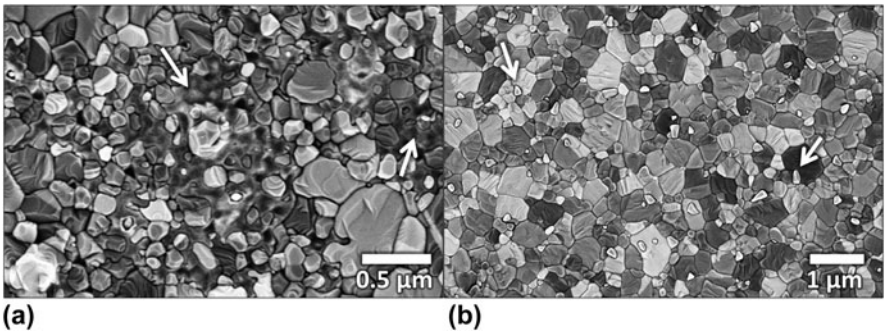


FIG. 5. SEM plan-view micrographs of second phases in (a) $BaTiO_3$ + 8 nm CuO + 2.2% BBO and (b) $BaTiO_3$ + 8 nm CuO, after annealing at 900 °C. Arrows indicate the location of second phases.

https://doi.org/10.1557/jmr.2016.89 Published online by Cambridge University Press

range. Adding BBO further increases the permittivity, yielding a 5× increase at room temperature.

In both samples containing CuO, there are two permittivity maxima as a function of temperature, each corresponding to phase transitions in $BaTiO_3$. The maxima are most pronounced when both CuO and BBO are present—this is interesting considering the similarity of microstructures seen in Figs. 1(h) and 1(i). Compared to the bulk Curie temperature, the ferroelectric–paraelectric phase transition shifts lower for pure $BaTiO_3$ thin films (T_C = ~100 °C), and higher for films with CuO (T_C = 165 °C) and CuO + BBO (T_C = 190 °C) additions. We attribute the lower temperature shift in pure $BaTiO_3$ to very fine grain sizes,[6,27] while the higher shifts for modified films are attributed to residual thermal expansion mismatch strain from the sapphire substrate.[11] Bulk ceramic studies of CuO additions to $BaTiO_3$ show that CuO can shift the ferroelectric transition, however, disagreement exists in the literature regarding the direction of this shift in bulk ceramics. Irrespective of their direction, all temperature shifts in bulk ceramics are limited to less than about 10 °C, substantially smaller than the ~50 °C increase observed in our flux-grown thin films. Consequently, the increases in T_C that we observe cannot be explained solely by chemical modification from fluxing agents, thus thermal strains likely play a predominant role.[15–17]

The absolute maximum in capacitance does not occur at the cubic–tetragonal (paraelectric–ferroelectric) transition as expected, but rather occurs near the lower temperature tetragonal–orthorhombic (ferroelectric–ferroelectric) transition. All samples with CuO show this peak, although the effect is most pronounced in those containing CuO + BBO. Ihlefeld et al. found a similar maximum in permittivity for $BaTiO_3$ with excess BaO on metal Cu foils heated at 1200 °C for 20 h.[28] We note that we do not observe this peak for $BaTiO_3$ + BBO films prepared without CuO regardless of grain size,[11] suggesting that CuO leads to this lower temperature maximum in a manner that we currently do not try to explain.

Capacitance–voltage (*C–V*) measurements, shown in Fig. 6(b) as relative tuning plots, serve as a probe for nonlinear dielectric properties and the relative contributions of ferroelectric domain wall motion to the material permittivity. Adding CuO to pure $BaTiO_3$ leads to a modest increase of tuning from 1.5:1 to 2:1, while addition of both CuO and BBO boosts the ratio to 3.5:1. We attribute the capacitance increase that accompanies CuO addition to an increase in grain size and density. Since the grain size of CuO and CuO + BBO samples are similar, some other mechanism must describe the large increase in capacitance that occurs when both BBO and CuO are present. We explain this observation by first considering that both films contain $BaAl_2O_4$. However, for the CuO modified film, the only source of Ba is the original and stoichiometric $BaTiO_3$. Consequently, $BaAl_2O_4$ formation will make the $BaTiO_3$ barium poor, which is associated with lower permittivity.[29] BBO additions can compensate for Ba loss to $BaAl_2O_4$ and preserve the desired 1:1 stoichiometry.

The second mechanism that impacts the dielectric response, and may be composition dependent, is aging, which can cause domain wall pinning and a reduction in extrinsic contributions.[30] To explore this possibility, the voltage-dependence of capacitance and loss were compared as a function of time and postanalysis heat treatments.

C–V measurements of the samples containing CuO, taken 2 mo after film deposition and annealing, showed signs of aging with distorted voltage dependencies.

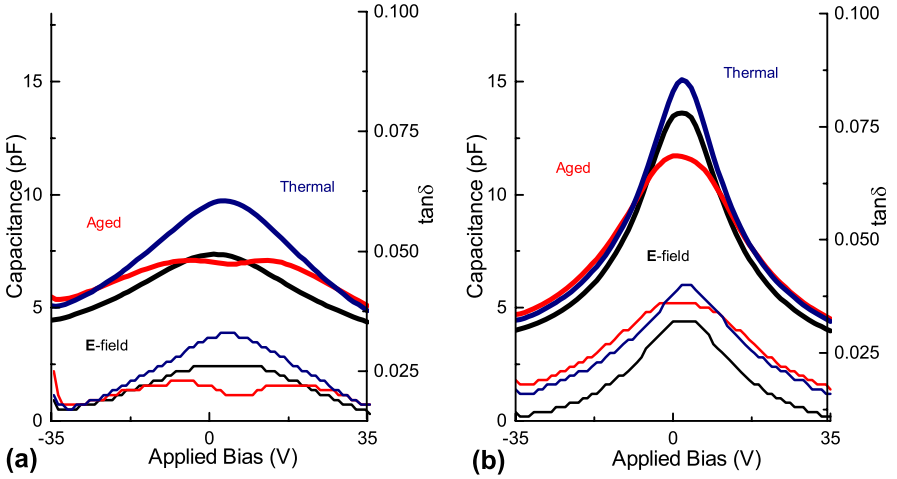


FIG. 7. Capacitance–voltage and dielectric loss measurements of (a) $BaTiO_3$ + 8 nm CuO and (b) $BaTiO_3$ + 8 nm CuO + BBO films after aging for 2 mo at ambient conditions (aged), and after de-aging at 250 °C for 30 min (thermal) or 1000 cycles of ±35 V (E-field). Measurements were performed at 1 MHz.

https://doi.org/10.1557/jmr.2016.89 Published online by Cambridge University Press

Figure 7 shows *C–V* for the same samples in the aged and recovered states. Recovery was accomplished by electric field cycling at room temperature or thermal annealing at 250 °C. All samples that contained CuO flux, regardless of BBO inclusion, exhibited aging phenomena, but the effect is most pronounced for samples containing only CuO. This is consistent with reports for $BaTiO_3$ ceramics showing that CuO incorporation leads to aging and reduced dielectric and nonlinear properties.[31] Current understanding suggests that Cu occupies the Ti site acting as an acceptor, and stabilizes oxygen vacancies in the material.[32] Over time, defect dipoles form and pin domain wall motion, which leads to property reductions.[33] De-aging by cycling ±35 V DC pulses for 1000 cycles or heating in air at 250 °C for 30 min then quenching in air increased room temperature capacitance and restored a symmetric *C–V* curve. All of the data in Fig. 6 represent measurements taken immediately after de-aging via heating above T_C. While there is no model presently available to explain this trend, it is possible that simultaneous composition modifications with Cu and B alter the extent to which Cu occupies the B-site, or interfere with the ability of defect dipoles to align with ferroelectric domains. In either case, the $BaTiO_3$ with BBO and CuO is more resistant to aging than $BaTiO_3$ with only CuO.

B. Microstructures on MgO

c-Sapphire substrates are convenient substrates by virtue of their wide current availability and low cost, however, they complicate understanding of the $BaTiO_3$–CuO–BBO system through substrate reactions that occur during annealing.[21] Changing the underlying substrate to MgO eliminates the role of Al diffusion and $BaAl_2O_4$ formation in the system. CuO and $BaTiO_3$ films were prepared on (100) MgO with identical processes to those on sapphire discussed previously. Figure 8 shows plan-view SEM images of the series of pure, CuO, and CuO + BBO $BaTiO_3$ on MgO after a 5 s etch in 5% HCl. Pure $BaTiO_3$ films on MgO are extremely fine grained. As seen in a similar sample series prepared on *c*-sapphire, adding CuO or CuO + BBO leads to substantial densification and grain growth, although the scale of the microstructure for all samples is greatly reduced (note the difference in scale bar for the images on MgO or values in Table I). The average grain size for pure $BaTiO_3$ on MgO is 58 nm. This increases to 90 nm with 8 nm CuO and then to 190 nm with BBO addition. This reduction in the efficacy could be due to negative interactions of the flux with the MgO substrate, however the only second phase peaks visible via XRD, shown in Fig. 9, are weak CuO. These results suggest that the inability to observe larger grain growth—in comparison to sapphire substrates—is the lack of Al in the system. Additionally, while the CuO grows $(\bar{1}11)$ on *c*-sapphire, CuO seems to have limited or no preferred growth direction on MgO. Just as with sapphire, second phases on the surface of the film are visible in SEM images shown in Fig. 10. It is interesting to note that the

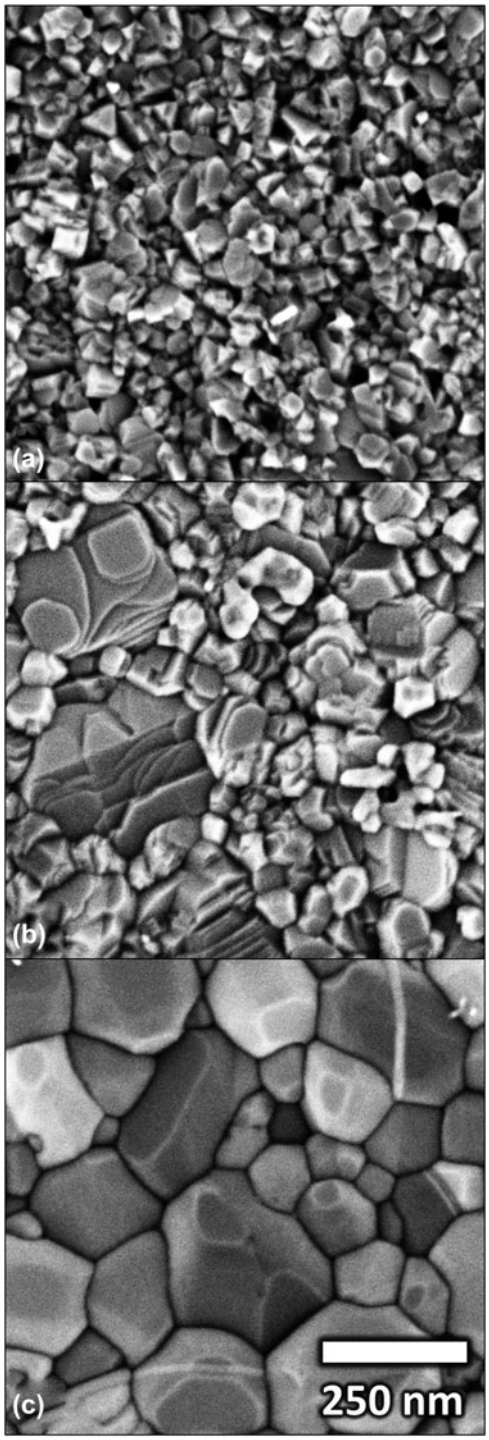


FIG. 8. SEM plan-view micrographs of (a) $BaTiO_3$, (b) $BaTiO_3$ + 8 nm CuO, and (c) $BaTiO_3$ + 8 nm CuO + BBO on MgO and annealed at 900 °C.

https://doi.org/10.1557/jmr.2016.89 Published online by Cambridge University Press

microstructure trends on MgO are identical to those on *c*-sapphire, but they occur on a different scale. Adding BBO to $BaTiO_3$ on MgO increases grain size, but the distribution is bimodal with large BT grains in a very fine matrix, and adding CuO greatly homogenizes the distribution. This observation leads again to the unexpected trend where incorporating Al_2O_3, a refractory oxide typically used to modify sintering behavior above 1150 °C,[34,35] enhances lower temperature transport in the $BaTiO_3$–B_2O_3–CuO system.

Figure 8(c) is a plan-view SEM image of $BaTiO_3$ modified with CuO and BBO where an equiaxed microstructure is achieved. Notable in this SEM image is linear contrast within the grains that are likely {111} twin lamellae. This contrast does not appear to be associated with abnormally large grains as is the case for $BaTiO_3$ + BBO on *c*-sapphire, nor is $BaAl_2O_4$ or $Ba_6Ti_{17}O_{40}$ present in XRD patterns (Fig. 9), both phases known to seed twinning.[22,36] CuO shares the monoclinic *C*2/*c* space group of $Ba_6Ti_{17}O_{40}$, however the structure of CuO is noticeably different, with no Ti–O octahedra that provide a topotactic interface between $Ba_6Ti_{17}O_{40}$ and $BaTiO_3$.[37]

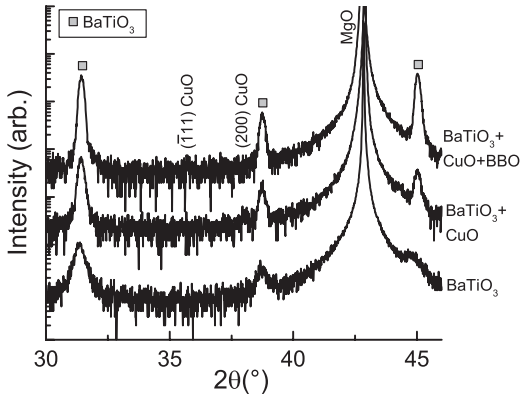


FIG. 9. XRD patterns of $BaTiO_3$ on MgO annealed at 900 °C with 8 nm CuO and 8 nm CuO + BBO additions.

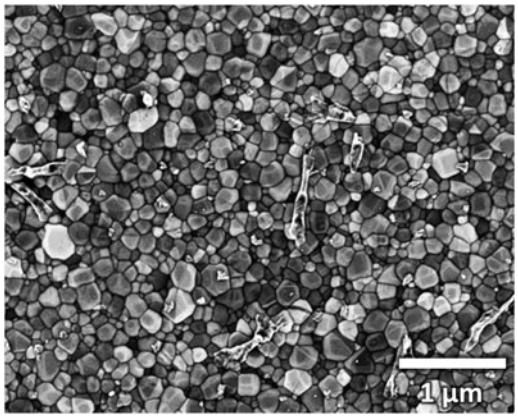


FIG. 10. SEM plan-view micrograph of $BaTiO_3$ + 8 nm CuO + 2.2% BBO on MgO and annealed at 900 °C showing second phase.

Derling et al. noted that $BaTiO_3$ with CuO and excess BaO led to elongated grains, stabilization of hexagonal $BaTiO_3$ at 150 °C lower than expected, and abnormal grain growth.[23] While Derling et al. did not discuss SEM sample preparation or characterize twinning behavior, the final microstructure is reminiscent of microstructures seen in TiO_2-excess $BaTiO_3$ ceramics, with elongated abnormally grown grains surrounded by a finer rounded grain matrix.[38–40] A later study of BaO–CuO in $BaTiO_3$ found similar abnormal grain growth and hexagonal phase behavior, and SEM micrographs of etched samples clearly demonstrate twin lamellae.[32] This understanding of CuO-modified $BaTiO_3$ ceramics leads to the hypothesis that the linear contrast visible in Fig. 8(c) originates from a similar composition-driven phenomenon.[41,42] We can add, however, that the composition effect is not solely associated with CuO since twinning in $BaTiO_3$ has been associated with a variety of composition changes.[22,39,41,43]

IV. CONCLUSIONS

CuO, with or without a BBO modifier, offers the ability to encourage significant grain growth and densification in $BaTiO_3$ films with restricted thermal budgets on a variety of substrates. Larger grain size and improved density enable large improvements in the dielectric properties and tuning. Films containing CuO (but no B_2O_3) exhibit strong aging that can be recovered by thermal anneals or field cycling. {111} twins are apparent in all samples containing CuO and/or BBO. On sapphire, BBO-modified films exhibited exaggerated grains that usually include a twin, however BBO-modified films with CuO show a more homogeneous grain size distribution. Microstructures on MgO exhibit universally smaller average grain size, likely due to the removal of Al_2O_3 from the system and the suppression of $BaAl_2O_4$ formation, but the addition of flux improves the density and leads to grain growth when compared to pure films.

ACKNOWLEDGMENTS

This material is based upon work supported by the NSF Center for Dielectrics and Piezoelectrics (NSF 1361503), the National Science Foundation Graduate Research Fellowship (NSF DGE-0946818), and the Army Research Office contract (W911NF1410285). Any opinion, findings, and conclusions or recommendations expressed in this material are those of the authors(s) and do not necessarily reflect the views of the National Science Foundation. The authors acknowledge the use of the Analytical Instrumentation Facility (AIF) at North Carolina State University, which is supported by the State of North Carolina and the National Science Foundation.

https://doi.org/10.1557/jmr.2016.89 Published online by Cambridge University Press

REFERENCES

1. S.M. Aygün, J.F. Ihlefeld, W.J. Borland, and J-P. Maria: Permittivity scaling in $Ba_{1-x}Sr_xTiO_3$ thin films and ceramics. *J. Appl. Phys.* **109**, 034108 (2011).
2. M.H. Frey, Z. Xu, P. Han, and D.A. Payne: The role of interfaces on an apparent grain size effect on the dielectric properties for ferroelectric barium titanate ceramics. *Ferroelectrics* **206**, 337–353 (1998).
3. T.M. Shaw, Z. Suo, M. Huang, E. Liniger, R.B. Laibowitz, and J.D. Baniecki: The effect of stress on the dielectric properties of barium strontium titanate thin films. *Appl. Phys. Lett.* **75**, 2129 (1999).
4. S.K. Streiffer, C. Basceri, C.B. Parker, S.E. Lash, and A.I. Kingon: Ferroelectricity in thin films: The dielectric response of fiber-textured $(Ba_xSr_{1-x})Ti_{1+y}O_{3+z}$ thin films grown by chemical vapor deposition. *J. Appl. Phys.* **86**, 4565 (1999).
5. G. Arlt, D. Hennings, and G. de With: Dielectric properties of fine-grained barium titanate ceramics. *J. Appl. Phys.* **58**, 1619 (1985).
6. Z. Zhao, V. Buscaglia, M. Viviani, M. Buscaglia, L. Mitoseriu, A. Testino, M. Nygren, M. Johnsson, and P. Nanni: Grain-size effects on the ferroelectric behavior of dense nanocrystalline $BaTiO_3$ ceramics. *Phys. Rev. B: Condens. Matter Mater. Phys.* **70**, 024107 (2004).
7. H. Kishi, Y. Mizuno, and H. Chazono: Base-metal electrode-multilayer ceramic capacitors: Past, present and future perspectives. *Jpn. J. Appl. Phys.* **42**, 1–15 (2003).
8. D. Prakash, B.P. Sharma, T.R. Rama Mohan, and P. Gopalan: Flux additions in barium titanate: Overview and prospects. *J. Solid State Chem.* **155**, 86–95 (2000).
9. R. Takahashi, Y. Yonezawa, M. Ohtani, M. Kawasaki, K. Nakajima, T. Chikyow, H. Koinuma, and Y. Matsumoto: Perfect $Bi_4Ti_3O_{12}$ single-crystal films via flux-mediated epitaxy. *Adv. Funct. Mater.* **16**, 485–491 (2006).
10. J.F. Ihlefeld, W.J. Borland, and J-P. Maria: Enhanced dielectric and crystalline properties in ferroelectric barium titanate thin films. *Adv. Funct. Mater.* **17**, 1199–1203 (2007).
11. D.T. Harris, M.J. Burch, J.F. Ihlefeld, P.G. Lam, J. Li, E.C. Dickey, and J-P. Maria: Realizing strain enhanced dielectric properties in $BaTiO_3$ films by liquid phase assisted growth. *Appl. Phys. Lett.* **103**, 012904 (2013).
12. D.T. Harris, P.G. Lam, M.J. Burch, J. Li, B.J. Rogers, E.C. Dickey, and J-P. Maria: Ultra-high tunability in polycrystalline $Ba_{1-x}Sr_xTiO_3$ thin films. *Appl. Phys. Lett.* **105**, 072904 (2014).
13. I. Burn: Flux-sintered $BaTiO_3$ dielectrics. *J. Mater. Sci.* **17**, 1398–1408 (1982).
14. D. Hennings and H. Schreinemacher: Method of producing a dielectric with perowskite structure and containing a copper oxide, United States Patent Office. U.S. Patent No. US4222885A, 1980.
15. D. Hennings and H. Schreinemacher: Method of producing a dielectric with perowskite structure and containing a copper oxide, United States Patent Office. U.S. Patent No. US4244830A, 1981.
16. T. Li, K. Yang, R. Xue, Y. Xue, and Z. Chen: The effect of CuO doping on the microstructures and dielectric properties of $BaTiO_3$ ceramics. *J. Mater. Sci.: Mater. Electron.* **22**, 838–842 (2010).
17. C-F. Yang: The influence of CuO–BaO mixture addition on the grain growth and dielectric characteristics of $BaTiO_3$ ceramics. *Ceram. Interfaces* **24**, 341–346 (1998).
18. ASTM International: *ASTM E112-13, Standard Test Methods for Determining Average Grain Size* (ASTM International, West Conshohocken, PA, 2013).
19. W. Zhang, K. Osamura, and S. Ochiai: Phase diagram of the BaO–CuO binary system. *J. Am. Ceram. Soc.* **73**, 1958–1964 (1990).
20. E.M. Levin and H.F. McMurdie: The system $BaO–B_2O_3$. *J. Am. Ceram. Soc.* **32**, 99–105 (1949).
21. M.J. Burch, J. Li, D.T. Harris, J-P. Maria, and E.C. Dickey: Mechanisms for microstructure enhancement in flux-assisted growth of barium titanate on sapphire. *J. Mater. Res.* **29**, 843–848 (2014).
22. D.T. Harris, M.J. Burch, J. Li, E.C. Dickey, and J-P. Maria: Low-temperature control of twins and abnormal grain growth in $BaTiO_3$. *J. Am. Ceram. Soc.* **98**, 2381–2387 (2015).
23. S. Derling, T. Müller, and H. Abicht: Copper oxide as a sintering agent for barium titanate based ceramics. *J. Mater. Sci.* **36**, 1425–1431 (2001).
24. J-B. Lim, S. Nahm, H-T. Kim, J-H. Kim, J-H. Paik, and H-J. Lee: Effect of B_2O_3 and CuO on the sintering temperature and microwave dielectric properties of the $BaTi_4O_9$ ceramics. *J. Electroceram.* **17**, 393–397 (2006).
25. M-H. Kim, Y-H. Jeong, S. Nahm, H-T. Kim, and H-J. Lee: Effect of B_2O_3 and CuO additives on the sintering temperature and microwave dielectric properties of $Ba(Zn_{1/3}Nb_{2/3})O_3$ ceramics. *J. Eur. Ceram. Soc.* **26**, 2139–2142 (2006).
26. A.M.M. Gadalla and J. White: Equilibrium relationships in the system $CuO–Cu_2O–Al_2O_3$. *Trans. Br. Ceram. Soc.* **63**, 57 (1964).
27. D. McCauley, R.E. Newnham, and C.A. Randall: Intrinsic size effects in a barium titanate glass-ceramic. *J. Am. Ceram. Soc.* **81**, 979–987 (1998).
28. J.F. Ihlefeld, P.R. Daniels, S.M. Aygün, W.J. Borland, and J-P. Maria: Property engineering in $BaTiO_3$ films by stoichiometry control. *J. Mater. Res.* **25**, 1064–1071 (2010).
29. J.K. Lee, K.S. Hong, and J.W. Jang: Roles of Ba/Ti ratios in the dielectric properties of $BaTiO_3$ ceramics. *J. Am. Ceram. Soc.* **84**, 2001–2006 (2001).
30. D.C. Lupascu, Y. Genenko, and N. Balke: Aging in ferroelectrics. *J. Am. Ceram. Soc.* **89**, 224–229 (2006).
31. Y.Q. Tan, J.L. Zhang, and C.L. Wang: Aging behaviours of CuO modified $BaTiO_3$ ceramics. *Adv. Appl. Ceram.* **113**, 223–227 (2014).
32. H.T. Langhammer, T. Müller, R. Böttcher, and H-P. Abicht: Crystal structure and related properties of copper-doped barium titanate ceramics. *Solid State Sci.* **5**, 965–971 (2003).
33. U. Robels and G. Arlt: Domain wall clamping in ferroelectrics by orientation of defects. *J. Appl. Phys.* **73**, 3454 (1993).
34. A. Young, G. Hilmas, S.C. Zhang, and R.W. Schwartz: Effect of liquid-phase sintering on the breakdown strength of barium titanate. *J. Am. Ceram. Soc.* **90**, 1504–1510 (2007).
35. Z.H. Wu, H.X. Liu, M.H. Cao, Z.Y. Shen, Z.H. Yao, H. Hao, and D.B. Luo: Effect of $BaO–Al_2O_3–B_2O_3–SiO_2$ glass additive on densification and dielectric properties of $Ba_{0.3}Sr_{0.7}TiO_3$ ceramics. *J. Ceram. Soc. Jpn.* **116**, 345–349 (2008).
36. V. Krasevec, M. Drofenik, and D. Kolar: Genesis of the (111) twin in barium titanate. *J. Am. Ceram. Soc.* **73**, 856–860 (1990).
37. V. Krasevec, M. Drofenik, and D. Kolar: Topotaxy between $BaTiO_3$ and $Ba_6Ti_{17}O_{40}$. *J. Am. Ceram. Soc.* **70**, C-193–C-195 (1987).
38. B. Lee, S. Chung, and S-J.L. Kang: Grain boundary faceting and abnormal grain growth in $BaTiO_3$. *Acta Mater.* **48**, 1575–1580 (2000).
39. B-K. Lee and S-J.L.L. Kang: Second-phase assisted formation of {111} twins in barium titanate. *Acta Mater.* **49**, 1373–1381 (2001).
40. B. Lee, S. Chung, and S.L. Kang: Necessary conditions for the formation of {111} twins in barium titanate. *J. Am. Ceram. Soc.* **83**, 2858–2860 (2004).
41. R.C. DeVRIES: Observations on growth of $BaTiO_3$ crystals from KF solutions. *J. Am. Ceram. Soc.* **42**, 547–558 (1959).
42. O. Eibl, P. Pongratz, and P. Skalicky: Crystallography of (111) twins in $BaTiO_3$. *Philos. Mag. Part B* **57**, 521–534 (1988).
43. O. Eibl, P. Pongratz, P. Skalicky, and H. Schmelz: Formation of (111) twins in $BaTiO_3$ ceramics. *J. Am. Ceram. Soc.* **70**, C-195–C-197 (1987).

https://doi.org/10.1557/jmr.2016.89 Published online by Cambridge University Press